THE ASTROPHYSICAL JOURNAL, 238:394–409, 1980 May 15

EMULSION CHAMBER OBSERVATIONS OF PRIMARY COSMIC-RAY ELECTRONS IN THE ENERGY RANGE 30–1000 GeV

J. NISHIMURA AND M. FUJII
Institute of Space and Aeronautical Science, University of Tokyo
T. TAIRA
Kanagawa University
E. AIZU AND H. HIRAIWA
Kanagawa Prefectural College
T. KOBAYASHI
Aoyama Gakuin University
K. NIU
Nagoya University
I. OHTA
Utsunomiya University
R. L. GOLDEN
Nex Mexico State University
AND
T. A. KOSS, J. J. LORD, AND R. J. WILKES
Visual Techniques Laboratory, University of Washington
Received 1979 September 4; accepted 1979 November 7

ABSTRACT

A series of emulsion exposures, beginning in Japan in 1968 and continued in the U.S. since 1975, has yielded a total balloon-altitude exposure of 98,700 m^2 sr s, nearly 10 times the exposure factor obtained by other experiments. The electron spectrum derived by combined data from all our chambers exposed from 1968 to 1976 is well represented by

$$J_e(E) = 1.6 \times 10^{-4}\left(\frac{100\ \text{GeV}}{E}\right)^{3.3\pm0.2} \Big/ \text{m}^2\ \text{sr s GeV}$$

in the energy range 30–1000 GeV. This result is in good agreement with our earlier results and with those of several other groups. We discuss our data in terms of several models of cosmic-ray propagation. Interpreted in terms of the energy-dependent leaky-box model, our electron spectrum results suggest a galactic electron residence time of $1.0(+2.0, -0.5) \times 10^7$ yr, which is consistent with the results from ^{10}Be observations. Additional chambers currently under analysis will allow us reliably to extend the spectrum beyond 1 TeV. We discuss the possibility that departures from smooth power-law behavior in the spectrum due to individual nearby sources will be observable in this energy range.

Subject headings: cosmic rays: general

I. INTRODUCTION

High-energy electrons in the galactic magnetic field lose energy through synchrotron radiation, producing the nonthermal galactic radio background. The energies of electrons are also decreased by inverse Compton collisions with low-energy photons of starlight and of the 2.7 K universal blackbody radiation. As the rate of energy loss of electrons in the interstellar medium is proportional to E^2, the energy spectrum of electrons should become steeper at higher energies. Thus measurement of the energy spectrum of primary electrons can give us information on the galactic magnetic and radiation fields as well as the confinement time of electrons in the Galaxy.

The intensity of cosmic electrons was found to be a few percent of the protons (Critchfield *et al.* 1952; Earl 1961; Meyer and Vogt 1961). In the energy region below 10 GeV, however, it is not possible to observe directly the interstellar electron spectrum because of solar modulation. Early measurements of cosmic electrons above 10 GeV were performed by several

groups (Bleeker *et al.* 1965; Daniel and Stephens 1965; Rubtsov 1965; Rubtsov and Zatsepin 1968). The data of Daniel and Stephens extends up to 300 GeV. Subsequently, many other experiments were performed to determine more precisely the primary electron spectrum above 10 GeV using a variety of experimental techniques.

The Chicago group (Müller and Meyer 1973) used an instrument which combined time-of-flight, Cerenkov, and shower detectors. Later (Hartmann, Müller, and Prince 1977; Prince 1979) they added a transition radiation detector to improve electron/proton discrimination. Others (Silverberg 1973; Meegan and Earl 1975; Silverberg 1976) have used electronic detectors differing in detail, but basically consisting of multilayer shower counters. Superconducting magnetic spectrometers have been used by Buffington *et al.* (1975) and Golden *et al.* (1977, 1979). Freier, Gilman, and Waddington (1977) used a detector combining emulsion and spark chambers. The measurements of Anand *et al.* (1968, 1970, 1973) and Nishimura *et al.* (1970) were made with nuclear emulsion stacks.

Inefficient rejection of background events (caused by hadrons and atmospheric gamma rays) is the main shortcoming of counter experiments, while superconducting magnetic spectrometers are limited by a maximum detectable momentum less than 100 GeV. Conventional emulsion stacks are limited in size by cost considerations, and thus yield low statistics. The emulsion chamber, the detector type used in the series of experiments summarized here, avoids many of these problems. Relatively small volumes of nuclear emulsion are needed, so large-acceptance detectors can be built at low cost. Positive identification of the incoming particles is possible because hadron, photon, and electron events leave distinctive signatures in the chamber. Detection efficiency is uniform and constant throughout the exposure. Electron energies are determined using the analytical three-dimensional shower theory (Nishimura 1964, 1967), whose validity has been checked against extensive Monte Carlo calculations (Taira 1979) and calibration experiments using Fermilab electron beams up to 300 GeV.

A series of emulsion chamber exposures, beginning in Japan in 1968, and continuing in collaboration with U.S. groups since 1975, has yielded a total balloon-altitude exposure of 98,700 m^2 sr s, nearly 10 times the exposure factor obtained by other experiments. Using this large statistical base, the primary electron spectrum can be plotted reliably from 30–1000 GeV. The experimental procedures used are detailed in § II, while the results obtained are presented in § III. The implications of the results regarding current models of cosmic-ray propagation inside the Galaxy are described in § IV. In particular, we discuss the fact that if the electron spectrum measurements are extended beyond 1 TeV, we might expect to see deviations from smooth power-law behavior due to nearby discrete sources (Shen 1970; Cowsik and Lee 1979; Nishimura *et al.* 1979).

II. EXPERIMENTAL PROCEDURE

Since 1968, four emulsion chambers have been exposed via balloon flight from Haranomachi and Sanriku, Japan, and three have been flown successfully from Palestine, Texas. In addition, small chambers of identical design were exposed for calibration purposes at Fermilab, using electron beams with energies of 50, 100, and 300 GeV. Table 1 summarizes the series of experiments.

a) Experimental Apparatus

An emulsion chamber consists of a stack of Pb or W plates, with nuclear emulsion plates and X-ray films inserted at intervals to sample the development of electromagnetic cascades produced in the metal plates. Cascades of energy greater than about 500 GeV will develop in 4–8 radiation lengths to the point where they leave spots on the X-ray film visible to the naked eye. Thus the X-ray films provide a convenient means of locating events, and serve as templates to permit rapid location of the showers in the emulsion plates. Once a shower has been picked up via the X-ray film, it can be traced back through the stack to its starting point, and the incoming particle can be identified. The emulsion chamber was originally developed to study high-energy cosmic-ray–hadron interactions (Kaplon *et al.* 1952; Minakawa *et al.* 1958), and the design has

TABLE 1

LIST OF BALLOON FLIGHTS

Flight	Area (m^2)	Time (min)	Average Altitude (mbar)	$S\Omega T$ (m^2 sr s)	Launch Site
1968	0.05	380	6.0	1826	Haranomachi, Japan
1969	0.05	267	7.0	1283	Haranomachi, Japan
1970	0.05	1136	6.0	5460	Sanriku, Japan
1973	0.20	833	8.0	19335	Sanriku, Japan
1976	0.40	1526	3.9	70841	Palestine, Texas
1977[a]	0.78	1760	4.4	159128	Palestine, Texas
1979[a]	0.80	1680	4.0	155790	Palestine, Texas

[a] Under analysis.

been modified in several ways for the electron spectrum experiments:

1. For convenience in tracing back events, it is desirable to have the photosensitive layers closely spaced near the top of the chamber, while thicker Pb layers are acceptable near the bottom. As shown in Figures 1*a* and 1*b*, the thickness of the Pb or W plates used in our chambers increased from 1 mm at the top to 5 mm at the bottom.

2. The use of two-sided emulsion plates permits accurate determination of the dip angle of the shower trajectory. To minimize transition effects in the shower development, emulsion layers are coated on the thinnest possible substrate. To minimize the number of background tracks in the emulsion, it is desirable to prepare the plates just before exposure. For example, in our 1968 experiment, only 14 days elapsed between manufacture and development of the emulsions.

3. High-sensitivity X-ray films are used in all layers.

4. Accurate alignment of the stack layers can be achieved through the use of carefully machined components and containers.

5. A remotely controlled flipper mechanism is used to keep the emulsion chambers inverted during ascent and descent of the balloon. This ensures that only particles recorded while the detector was at float altitude will trace back in the correct manner.

Figure 1*a* shows the chamber used in 1968, with area 20×25 cm^2 and total thickness 8.2 radiation lengths (r.l.). The chamber had 18 photosensitive layers, each containing a glass-based Fuji ET7A nuclear emulsion plate and two Sakura Type N X-ray films. Figure 1*b* shows the detector used in 1976, with area 40×50 cm^2 and thickness 8.2 r.l. Each of the 24 film layers contains two Sakura Type N X-ray films and a nuclear emulsion plate. The emulsion plates were methacrylate plastic 0.08 cm (800 μm) thick, with 100 μm layers of Fuji ET7B emulsion coated on both sides. The plates were slightly overdeveloped by using amidol-bisulfite developer at 20° C for 40 minutes, which yielded a developed grain density of 35–40 grains per 100 μm of relativistic track. Thus even minimum-ionizing particles could be readily traced back from plate to plate without ambiguity.

b) Scanning, Traceback, and Event Identification

Two methods were used for locating events. For electron showers with energy above 500 GeV, the X-ray films in each layer of the chamber are scanned on a light table. The use of two films per layer permits rapid elimination of random spots due to pressure marks.

The efficiency for detecting electromagnetic showers in emulsion chambers using X-ray films has been studied by several groups (Fujimoto *et al.* 1960; Ohta 1971; Ohta *et al.* 1979). These workers found that the detection efficiency is essentially 100% beyond a certain energy threshold, and below this falls off rather rapidly. These conclusions are confirmed by exposures in which the events were located by both microscope and X-ray film scanning in the same energy region. Both procedures gave the same flux of atmospheric γ-rays (Nishimura 1961; Takahashi, Iwai, and Ohta 1977). The detection threshold for the X-ray film varies according to the accumulated background fog in the film. Freshly manufactured film yields a threshold around 300–400 GeV, while showers below 600 GeV are often difficult to detect in film stored for 1 year.

Once a shower has been found the corresponding tracks in the emulsion plate are quickly located. To extend our sample to lower energies, the emulsion plates are directly scanned using microscopes. Since lower-energy electrons are more abundant, only a fraction of the chamber area need be scanned to obtain an adequate data sample. Microscope scans of a given area were performed by two or more observers. Showers were recorded which had, within a radius of 100 μm, more than 4 electrons at a depth of 2.0 r.l., corresponding to a minimum energy of 30 GeV. Similarly, showers were recorded which had more than six electrons at a depth of 2.55 r.l., or 10 electrons at a depth of 3.72 r.l., for thresholds of 60 and 150 GeV, respectively (Fig. 2). The detection efficiency for such events depends upon the fluctuations in the number of electrons at a given depth. The detailed behavior of electron showers in the emulsion chamber was studied by a Monte Carlo simulation. The results of this simulation indicate a detection efficiency greater than 95%.

The detection efficiency for microscope scanning was also tested by scanning emulsion plates exposed to the 100 GeV electron beam at FNAL. A scan was made for showers with more than 8 tracks within a circle of 100 micron radius at depths of 3.42 and 4.30 radiation lengths. In the first scan 40 events were detected, and no further events were detected in the second scan. The distribution of the number of tracks at each depth was similar to that predicted by the Monte Carlo calculation, and thus confirmed the detection efficiency predicted by the Monte Carlo simulation.

The following geometric cuts were applied: (1) Event trajectories were required to pass through the top and bottom emulsion plates. (2*a*) Events picked up on X-ray film were required to have a zenith angle of less than 60°. (2*b*) Events picked up by microscope were required to have a zenith angle less than 45°.

Showers were traced back to their starting point, and the incoming particle track, if any, was traced to the top of the stack. The traceback process was facilitated by careful alignment of the plates, and the use of heavy primary particles as reference tracks. This method yielded a relative positioning accuracy for adjacent plates of about 10 μm.

The identity of the incoming particle could be determined by examining the details of shower development. Electron showers start from a single charged track which, with about 90% probability, produces a pair within 1 r.l. of the top of the chamber. A photon shower starts from a pair, with no visible primary track. Showers associated with hadrons have

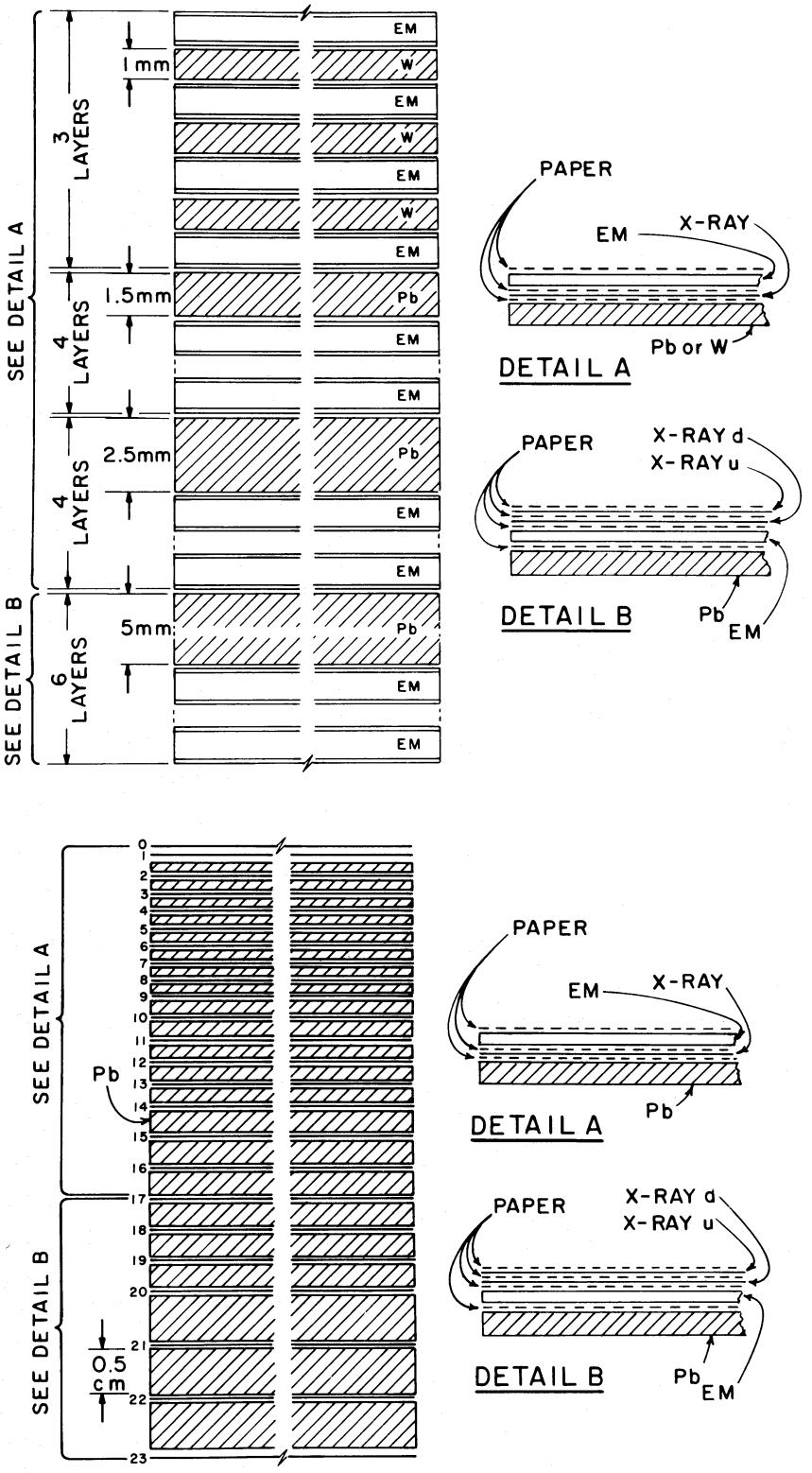

FIG. 1.—Emulsion chamber configuration for 1968 flight (*top*) and 1976 flight (*bottom*)

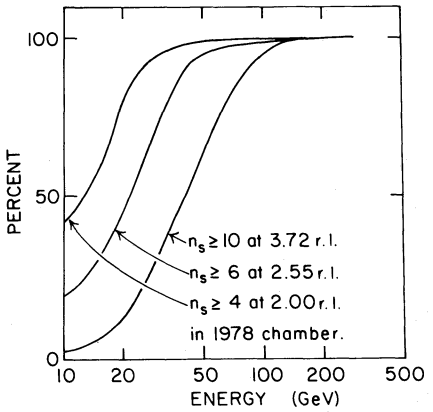

FIG. 2.—Electron shower scanning efficiencies, from a Monte Carlo simulation. Curves give the probability, as a function of energy, that an electron shower will contain at least the indicated number of tracks (within a circle of radius 100 μm) at the specified depths in the chamber.

several distinguishing characteristics. First, electron showers must have their starting points near the top of the chamber, while nuclear interactions are almost uniformly distributed along the thickness of the chamber. Second, the high mean charged and neutral multiplicities of hadronic interactions in the energy range considered means nuclear interactions are characterized by the appearance of many secondaries at the starting point, and a multicore structure in the shower at greater depths. Only hadronic interactions originating at the top of the chamber and producing one or three charged prongs could be mistaken for electron events. Using data from accelerator emulsion exposures (Konishi *et al.* 1976), we estimate that about 2% of hadronic interactions in the energy range 100–1000 GeV have these characteristics. However, the emulsion chamber technique tends to yield an enhanced sample of such interactions, since events are selected according to the total energy going into γ-rays, ΣE_γ, and near threshold this "trigger" criterion favors events with low charged multiplicity. For example, an experiment using chambers similar to ours, exposed to 303 GeV protons at Fermilab (Fuchi *et al.* 1978; Tasaka 1979), found that one- and three-prong topologies constitute about 20% of all events found with $\Sigma E_\gamma > 80$ GeV (12 out of 70 events). A cosmic-ray experiment using similar techniques (Sato *et al.* 1976) found a slightly lower proportion (two out of 15 events) for $\Sigma E_\gamma > 500$ GeV. Thus the observed percentage of one- and three-prong interactions shows little change in this energy range, although a slight decrease is expected as a result of the higher average multiplicity in the TeV region. In our 1976 exposure, we found eight electrons and 25 proton-induced events within 1 r.l. of the tops of the chambers. Three of the proton events had one or three charged prongs, which is entirely consistent with the three or four events expected on the basis of the experiments just cited. However, all of these low-multiplicity events, those of Sato *et al.* (1976) and Tasaka (1979), as well as ours, showed features distinctly different from those expected of electron-initiated showers: multicore shower structure, late development of showers due to γ-rays from π^0 decay, and angular distributions consistent with transverse momenta on the order of several hundred MeV/c. It is thus quite unlikely that our sample of electrons is contaminated by more than 10% with misidentified proton interactions.

c) Energy Determination

Electron energies were determined by counting the number of electrons in each emulsion plate within a circle of radius 100 μm centered on the shower axis. These data can be related to the electron energy through the three-dimensional analytical shower theory (Nishimura 1967).

The shower theory gives average features of electromagnetic cascades in homogeneous materials such as pure lead or emulsion. Emulsion chambers are inhomogeneous, since the lead is "diluted" by the presence of the film layers. A calculation has been performed taking into account such inhomogeneity (Nishimura 1964), and a Monte Carlo simulation using the actual chamber configuration (Taira 1979) agrees quite well with this modified theory. Shower transition curves generated from the modified theory and used in the analysis of the 1976 stack data are shown in Figure 3. As a final check, emulsion chambers identical to the 1976 balloon flight stacks, except for smaller transverse dimensions, were prepared and exposed to Fermilab electron beams. Energies of 50, 100, and 300 GeV were used, and the results obtained are also shown in Figure 3. The data agree well with the theory within experimental errors.

An important result of the analytical shower theory

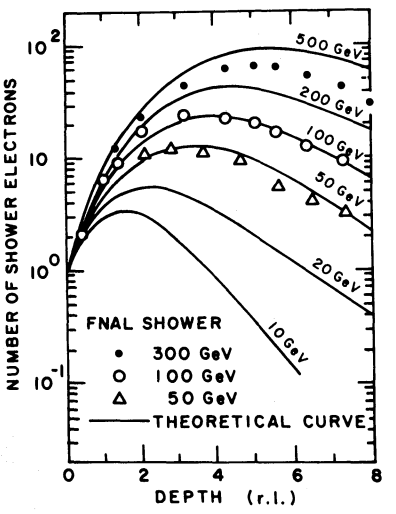

FIG. 3.—Results of the Fermilab calibration exposures. Data points indicate the average number of shower particles counted within a circle of 100 μm radius as a function of depth in the emulsion chamber, for 50, 150, and 300 GeV electrons. Also shown are shower development curves calculated using the three dimensional analytic shower theory (Nishimura 1964).

TABLE 2

ELECTRON SPECTRUM DATA

Energy bin (GeV)	$\langle E \rangle$	$S\Omega T$ (m^2 sr s)	N	Flux (J) (m^2 sr s GeV)$^{-1}$	$E^3 \times J$
800–1500	1077	9.87×10^4	4	$5.79 \pm 3.34 \times 10^{-8}$	72.3 ± 41.7
600–800	688	6.33×10^4	5	$3.95 \pm 1.98 \times 10^{-7}$	128.6 ± 64.5
300–500	382	5784	3	$2.59 \pm 1.83 \times 10^{-6}$	144.6 ± 102.0
200–300	244	5792	6	$1.04 \pm 4.7 \times 10^{-5}$	151.1 ± 67.6
150–200	172	1679	3	$3.57 \pm 2.5 \times 10^{-5}$	181.7 ± 128.4
100–150	121	1679	8	$9.53 \pm 2.7 \times 10^{-5}$	168.8 ± 63.8
80–100	88.8	682	4	$2.93 \pm 1.69 \times 10^{-4}$	205.2 ± 118.5
60–80	68.8	682	5	$3.67 \pm 1.84 \times 10^{-4}$	119.5 ± 59.8
60–100	75.8	682	9	$3.30 \pm 1.2 \times 10^{-4}$	143.7 ± 50.8
30–50	37.9	69.8	6	$4.30 \pm 1.9 \times 10^{-3}$	234.0 ± 104.6

is that the integrated track length is the optimal parameter for energy determination:

$$Z_\pi(r \leq 100\mu) = \int_0^\infty dt \int_0^{100\,\mu m} \Pi(r, t) 2\pi r dr\,, \quad (1)$$

where Π is the number density of shower electrons at radius r and depth t. The integrated track length is expected to be free of serious fluctuations and directly proportional to shower energy, as discussed in detail in Appendix A. The results of the Monte Carlo calculation and the Fermilab calibrations verify these features.

In the experiments described here, we estimated the integrated track length by numerical integration of the track counts in each layer:

$$Z_\pi = \sum_i a_i N_i\,, \quad (2)$$

where N_i is the number of electrons within 100 μm of the shower axis in emulsion plate i, and a_i is the weight parameter for layer i which reflects the actual distance, in radiation lengths, traversed by the shower in traveling from one plate to another in the chamber. The a_i are therefore dependent on the zenith angle of the shower. A correction for tracks escaping from the chamber is made by adding to the track length produced in the chamber an additional track length which would be expected from the shower theory to be produced in an infinitely deep chamber. We estimate the precision in individual energy determinations to be about 15% for electrons of energy greater than 50 GeV, using the results of the Fermilab calibration.

III. RESULTS

a) *Electron Spectrum*

The differential electron spectrum data obtained by combined results from all emulsion chambers exposed from 1968 to 1976 are listed in Table 2 and shown in Figure 4, along with results from other groups. The energy value for each electron has been corrected for energy loss in the overlying atmosphere, taking into account the approximate slope of the energy spectrum. It is to be noted that corrections calculated using the simple average energy loss of a single electron would be overestimated, as discussed in Appendix B. The resulting spectrum is well represented by

$$J(E) = 1.6 \times 10^{-4} (100\ \text{GeV}/E)^{3.3 \pm 0.2} / \text{m}^2\ \text{s sr GeV}\,. \quad (3)$$

Our data are limited to the region above 30 GeV.

The conventional plot shown in Figure 4 obscures the substantial differences between the results of various groups. The data are replotted in Figure 5, with the vertical scale expanded by a factor of E^3. The presence of unresolved systematic errors in some of the published data is obvious.

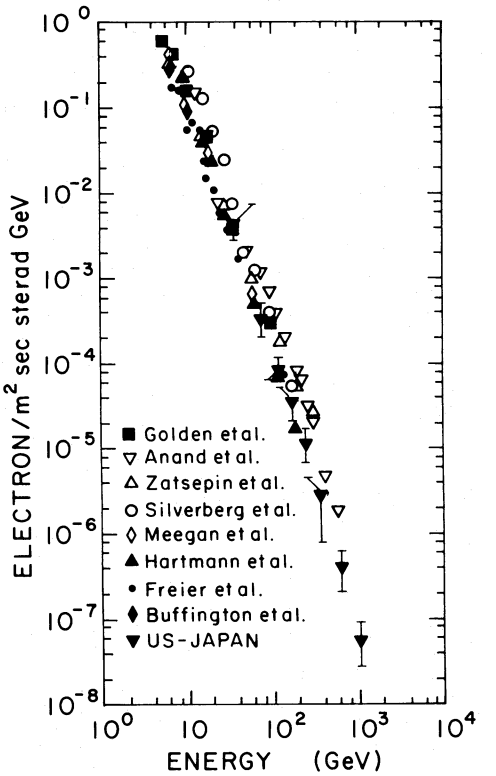

FIG. 4.—Differential energy spectrum of primary electrons (conventional plot).

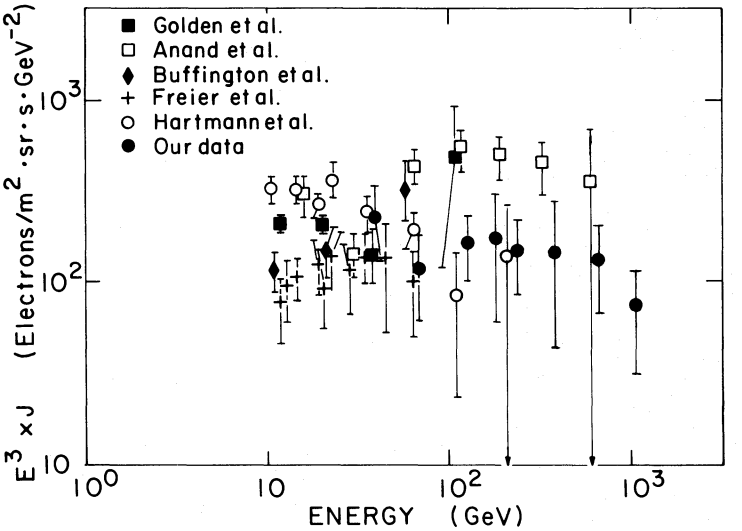

FIG. 5.—Differential energy spectrum of primary electrons, with flux values multiplied by E^3 to expand the vertical scale

Only four other experiments have produced data above 100 GeV. The Chicago group (Müller and Meyer 1973) results indicating a spectral slope of approximately 2.8 have been withdrawn, and the latest data from this group (Hartmann, Müller, and Prince 1977), extending only to 200 GeV, indicates a result compatible with ours. Anand, Daniel, and Stephens (1968, 1973), using nuclear emulsion stacks with a relatively small net exposure factor, obtained a spectrum with intensity greater than ours by a factor of about 3. Several comments can be made regarding the latter experiment. First, their energy determination depends upon a Monte Carlo simulation above 30 GeV (Anand 1973). We exposed a chamber of identical configuration to 300 GeV electrons at Fermilab, and the showers were analyzed using their criteria. The results show that their simulation overestimates shower energy by a factor of 1.2–1.3. Our Monte Carlo simulation agrees with this conclusion. Second, their correction for overlying atmosphere does not take into into account the effect of the spectral slope, and thus overestimates the energy loss by another factor of 1.1. The flux is therefore overestimated by a factor of about 2, which would bring their data into line with ours.

b) Atmospheric γ-Ray Spectrum

In our emulsion chambers, γ-ray events are picked up in the course of data reduction, and the gamma spectrum thus obtained is shown in Figure 6. Essentially all such photons are due to neutral pions from nuclear interactions in the overlying atmosphere, and thus the flux should be proportional to the atmospheric depth at balloon altitude. The data shown, combined from the results of several of our balloon flights, have been normalized to 4 g cm^{-2}, and are well represented by

$$J_\gamma(E) = 1.20 \times 10^{-4} \times (100\ \mathrm{GeV}/E)^{2.75 \pm 0.10}/\mathrm{m}^2\ \mathrm{sr\ s\ GeV}\ . \quad (4)$$

Using recent accelerator data on nuclear interactions and the measured primary cosmic-ray hadron flux (Ryan *et al.* 1972), it is possible to calculate the expected secondary particle flux with reasonable accuracy. Badhwar, Stephens, and Golden (1977) and Murakami *et al.* (1977) find fair agreement between the calculated and observed high-energy muon spectra. Orth and Buffington (1976) used this approach to estimate the flux of secondary positrons in the atmosphere. Murakami *et al.* (1979) also calculated the flux

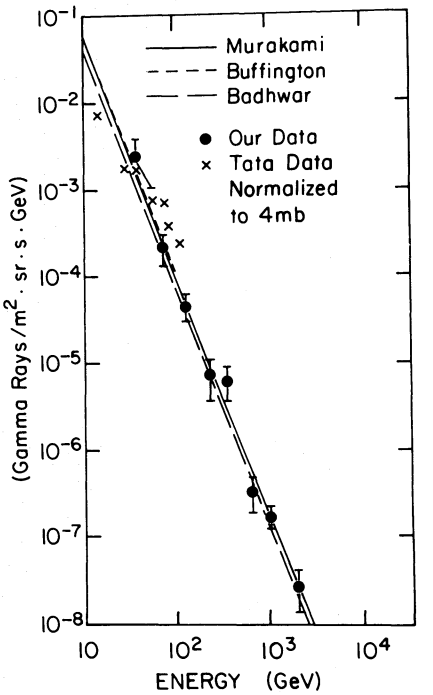

FIG. 6.—Differential energy spectrum of atmospheric γ-rays, normalized to a pressure depth of 4 mbar.

of atmospheric gamma rays, and at 4 g cm^{-2} obtain

$$J_\gamma(E) = 1.19 \times 10^{-4} \times (100\ \mathrm{GeV}/E)^{2.72}\ \mathrm{m^2\ sr\ s\ GeV^{-1}}. \quad (5)$$

While Badhwar, Stephens, and Golden (1977) and Orth and Buffington (1976) did not explicitly calculate the gamma flux, one can derive the expected spectrum from their published pion spectra. Figure 6 shows that our data agree fairly well with these calculations.

Another approach, which does not require knowledge of production cross sections or the primary hadron flux, depends on the assumption of charge symmetry in the production of pions. Since muons result from the decay of charged mesons, and gamma rays are the decay products of neutral pions, the γ-ray flux can be derived from the observed sea-level or underground muon flux. The only parameter which must be extrapolated from the lower-energy accelerator data is the K/π ratio. Such calculations have been performed by several authors, and the results agree quite well with our experimental data and with the theoretical curves in Figure 6, while the gamma spectrum of Stephens (1970) disagrees with the predicted spectrum by a factor of about 2 for $E > 30$ GeV. Stephens (1970) used the scattering method, calibrated by an accelerator experiment, for energy determinations below 30 GeV, while above 30 GeV they used the track-counting method, based upon their Monte Carlo calculations. This disagreement is due to the energy overestimate described in § III*a*.

Since the γ-ray events in our chambers are located and analyzed in exactly the same way as the electron events, the agreement between our observed gamma spectrum and the independently calculated spectra provides a significant check on the reliability of our experimental technique.

c) Checks on Event Identification

Although there is little possibility of error in particle identification in our experiment, since each cascade in our emulsion chambers is traced back to its starting point, our analysis procedures yield two additional checks on identification efficiency: the zenith angle distribution and the shower starting point distribution.

For primary electrons, the zenith angle distribution will be isotropic, and thus for a plane detector the observed angular distribution will be

$$F_e(\cos\theta)d\cos\theta \propto \cos\theta d\cos\theta, \quad (6)$$

neglecting the effect of the finite detector size. The distribution for atmospheric γ-rays should be

$$F_\gamma(\cos\theta)\mathrm{d}\cos\theta \propto d\cos\theta \quad (7)$$

since the γ-rays are produced in the overlying residual atmosphere and thus have a sec θ enhancement relative to the isotropic primary hadron flux.

The distribution for primary hadrons should be similar to that of γ-rays, since the path length in the chamber (hence detection probability) is proportional to sec θ. However, the hadron zenith angle distribution will be distorted by detection biases, since our detection efficiency is a complex function of the interaction location and fraction of energy going into pion production.

Zenith angle distributions for the three classes of events are shown in Figure 7, and are in good agreement with the expected forms.

The shower starting-point distribution for γ-rays is also used as a check on our identification efficiency, and will have the approximate form

$$\exp(-\sigma_0 t)dt, \quad (8)$$

where t is measured in radiation lengths and $\sigma_0 = 7/9$. For electrons, the calculated shower starting point distribution is

$$\exp\{-[(\sigma_0/2)t^2 \ln(E_0/E)]\}\sigma_0 t \ln(E_0/E)dt, \quad (9)$$

where E_0 is the primary electron energy, and E is the threshold energy for pair production. For hadrons, the interaction mean free path is about 30 r.l. in Pb, so the chamber thickness is only a fraction of an interaction

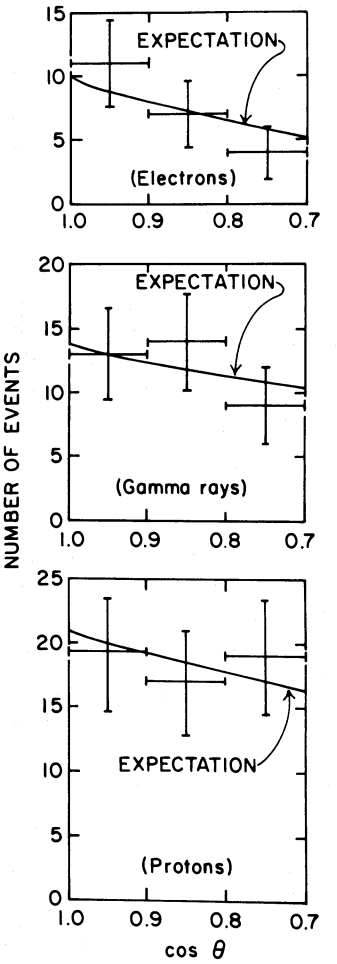

FIG. 7.—Angular distributions for events classified as electrons, γ-rays and protons. Curves indicate the expected distributions.

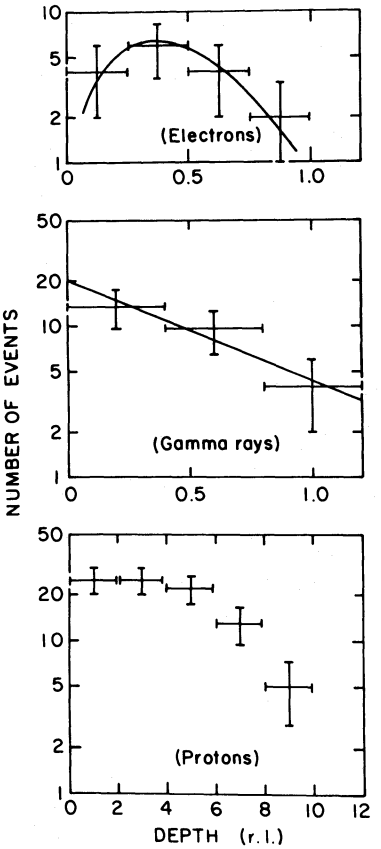

FIG. 8.—Shower starting-point distributions for events classified as electrons, γ-rays and protons. Curves indicated the expected distributions.

length, and the starting-point distribution should be almost uniform in t. In Figure 8 we show the observed starting-point distributions, which show reasonable agreement with the expected forms, providing a further check on the reliability of our method.

IV. ASTROPHYSICAL IMPLICATIONS OF RESULTS

As noted in § I, the dominant energy-loss mechanisms for high-energy electrons propagating through the interstellar medium are synchrotron radiation and inverse Compton scattering, both of of which produce energy-loss rates proportional to E^2. Thus the mean lifetime of a cosmic-ray electron with respect to energy loss is proportional to $1/E$. For sufficient energy, this lifetime becomes shorter than the lifetime with respect to leakage from the Galaxy, and the slope of the observed electron spectrum should steepen by about one unit relative to that of the source spectrum. The energy at which the slope changes, and the detailed nature of the transition, are dependent upon the propagation mechanism, as well as the strength of the galactic magnetic field, and the intensity of starlight and the 2.7 K radiation, so that accurate measurement of the primary electron spectrum can have considerable astrophysical significance.

In addition to direct measurements of the electron flux near the Earth by experiments of the type described here, the synchrotron radiation emitted by electrons passing through distant regions of the Galaxy can be observed as diffuse nonthermal radio-frequency radiation, and the electron spectrum can be inferred if the magnetic field in the source region is known. Unfortunately, at the present time such measurements can observe only a limited frequency range, corresponding to a limited maximum electron energy; moreover, apparent conflicts exist between results on intensity obtained by the two experimental techniques (Badhwar, Daniel, and Stephens 1977).

At very high energies, e.g., above 1 TeV, the electron propagation lifetime is so short that only a few cosmic-ray sources could contribute to the observed flux (Shen 1970; Cowsik and Lee 1979; Nishimura *et al.* 1979). Thus one expects fluctuations in the electron-energy spectrum reflecting the presence of these discrete sources. Using information on the age and distance of known supernova remnants near the solar system, one could determine which source may contribute electrons most efficiently to a given energy range, and thus correlate individual sources with features of the primary electron spectrum. Thus accurate measurement of the electron spectrum in the TeV region takes on added significance. This new development is discussed in more detail in § IV*b*.

a) Electron Flux from Nonthermal Radio Observations

The intensity spectrum for radiation emitted by a relativistic electron is peaked at the frequency

$$\nu_m = 1.2 B_\perp \left(\frac{E}{mc^2}\right)^2 \text{MHz}\,, \qquad (10)$$

where $B_\perp$ is in gauss.

Radio data exist up to 15 GHz, which corresponds to a mean electron energy of $\sim$15 GeV, assuming $B_\perp = 3$ microgauss and the spectral index $\gamma \sim 3$. For an electron spectrum of the form dE/E^γ, the synchrotron intensity is proportional to $B_\perp^{(\gamma+1)/2} \nu^{(\gamma-1)/2} d\nu$. Hirabayashi (1974) finds that the slope of the frequency spectrum is 0.95 in the 10 GHz region. It is difficult to estimate the errors in this value, but the author suggests ± 0.1 or more (Hirabayashi 1979). This implies an electron spectral index of $\gamma = 2.90 \pm 0.2$ in the 10 GeV region. However, the electron intensities inferred from the radio observations are 5–10 times greater than those obtained from direct measurements. This disagreement suggests the following possibilities: (1) the effective galactic magnetic field for production of synchrotron radiation is in fact larger than the generally accepted value of 3–4 microgauss; (2) the local electron flux is smaller than the average flux elsewhere in the Galaxy; (3) a combination of (1) and (2).

Several authors have discussed possibility (1) using the following arguments (Cowsik and Mitteldorf 1974; Freier *et al.* 1977). The galactic magnetic field is derived from Faraday rotation measurements or from

observations of the Zeeman effect, both of which are proportional to B; the value thus obtained represents $\langle B \rangle$ for the region examined. However, the intensity of synchrotron radiation is proportional to

$$B^{(\gamma+1)/2} \rightarrow B^2 \quad \text{for } \gamma = 3\,, \tag{11}$$

so that radio observations effectively sample the root-mean-square field. Thus large fluctuations in the magnetic field would increase the effective field for production of synchrotron radiation, bringing the radio observations into agreement with the electron flux data. In this case the synchrotron loss would dominate the inverse Compton loss, and the electron lifetime due to energy loss would be decreased by a factor of 2–3.

Regarding the second possibility, recent data from *SAS 2* (Fichtel *et al.* 1975) and *COS B* (Bennett *et al.* 1977) indicate the existence of cosmic-ray confinement domains on the order of 1 kpc (Stecker and Jones 1977). Also, the γ-ray spectrum observed by *COS B* seems to suggest a dominant contribution from bremsstrahlung, rather than from pion decay from nuclear interactions, indicating a higher e/p ratio in remote regions than that observed near the solar system (Paul *et al.* 1978). Thus the directly observed local electron flux may differ substantially from that in the synchrotron-radiating regions.

b) *Models of Propagation*

Several models have been proposed to describe cosmic-ray propagation in the Galaxy, motivated by attempts to fit existing data on the spectra of heavy primaries of different species assuming the same simple power-law source spectrum (Cowsik and Wilson 1973; Webber 1973; Ramaty 1974; Reames 1974). Recent data on the flux of diffuse γ-rays also provide important clues regarding the propagation mechanism. The electron spectrum provides a critical test for such models. We will discuss two classes of models, the energy-dependent homogeneous leaky-box model, and the diffusion model.

Electrons lose energy at the rate

$$-\frac{dE}{dt} = bE^2\,,$$

with

$$b = \frac{32\pi}{9}\left(\frac{e^2}{mc^2}\right)^2 \frac{c}{(mc^2)^2}\left(\frac{B^2}{8\pi} + \rho\right); \tag{12}$$

B is the magnetic field strength, and ρ is the energy density of photons (starlight plus 2.7 K blackbody radiation). If one assumes $B = 3$ microgauss, we have $b = 10^{-16}\,(\text{GeV s})^{-1}$. Using this value for b, the lifetime with respect to energy loss is then

$$T_e \approx \frac{1}{bE} = \frac{3 \times 10^8}{E(\text{GeV})}\,\text{yr}\,. \tag{13}$$

The energy-dependent leaky-box model has been discussed in connection with the electron spectrum (Silverberg and Ramaty 1973; Ormes and Freier 1978). The differential equation governing the electron spectrum $J(E, t)$ is

$$\frac{\partial J}{\partial t} + \frac{J}{\tau} - \frac{\partial bE^2 J}{\partial E} = Q(E)\,, \tag{14}$$

where τ is the leakage lifetime and Q is the source spectrum.

The main feature of the model is the use of an energy-dependent leakage lifetime to explain the observed gradual decrease of the L/M ratio with increasing energy. Two parameters are introduced, τ_0 and δ, and the leakage lifetime is given by

$$\begin{aligned} \tau &= \tau_0 (E/5)^{-\delta} && \text{for } E \gtrsim 5\ \text{GeV}\,, \\ &= \tau_0 && \text{for } E \lesssim 5\ \text{GeV}\,, \end{aligned} \tag{15}$$

where E is the energy in GeV.

A solution of equation (14) can be derived (Silverberg and Ramaty 1973):

$$J = \frac{1}{E^2}\int_0^{1/bE} (1/E - bt)^{-2} Q[(1/E - bt)^{-1}] \times \exp\left\{-\left[\frac{1 - (1 - bEt)^{1-\delta}}{\tau(1-\delta)bE}\right]\right\} dt \quad \text{for } E \gtrsim 5\ \text{GeV}\,, \tag{16}$$

and if we assume a source spectrum of the form $Q = 1/E^\gamma$, one has

$$\begin{aligned} J &= \frac{1}{E^2}\int_0^{1/bE} (1/E - bt)^{\gamma-2} \times \exp\left\{-\left[\frac{1 - (1 - bEt)^{1-\delta}}{\tau(1-\delta)bE}\right]\right\} dt \\ &= \frac{\exp\{-[1/\tau(1-\delta)bE]\}}{b(\gamma-1)E^{\gamma+1}} \times F\left(1; \frac{\gamma-1}{1-\delta}; \frac{1}{\tau(1-\delta)bE}\right), \end{aligned} \tag{17}$$

where F is the confluent hypergeometric function. The essential features of the solution (17) can be seen as follows. At low energies, T_e is longer than τ, and thus the electron lifetime is essentially determined by leakage, as with the other cosmic-ray components. Thus the low-energy electron spectrum has the form

$$J_e \approx \tau Q = \frac{\tau_0 5^\delta}{E^{\gamma+\delta}}\,. \tag{18}$$

At higher energies, $T_e < \tau$ so that $J_e \approx T_e Q$; more precisely,

$$J_e \approx \frac{T_e Q}{\gamma - 1} = \frac{1}{b(\gamma-1)E^{\gamma+1}}\,, \tag{19}$$

and the change in the spectral index over the energy region $E \ll E_c$ to $E \gg E_c$ is

$$(\gamma + 1) - (\gamma + \delta) = 1 - \delta\,, \qquad (20)$$

where E_c is defined by the formula

$$\frac{T_e}{\gamma - 1} = \tau; \quad E_c = [b(\gamma - 1)\tau_0]^{-(1/1-\delta)} 5^{-(\delta/1-\delta)}\,. \qquad (21)$$

At low energies, there is considerable spread in the measurements, but the data can be fitted reasonably well by a spectral index of 2.8 ± 0.2. At energies above 100 GeV, our data give an index of 3.3 ± 0.2. We can thus obtain the value of δ from equation (20):

$$1 - \delta = 0.5 \pm 0.3; \quad \delta = 0.5 \pm 0.3\,. \qquad (22)$$

This value is consistent with that obtained from the analysis of heavy-primary spectra (Smith *et al.* 1973; Juliusson *et al.* 1975; Caldwell 1977; Lezniak *et al.* 1977; Ormes and Freier 1978; Orth *et al.* 1978).

From the data of Figure 5, the spectrum appears to bend gradually between 50 and 200 GeV. Using these energy values, formula (21) yields $\tau_0 = 5 \times 10^6$–3×10^7 yr for $\delta = 0.2$–0.7. In fact, as shown in Figure 9, a reasonable fit between the spectral function (17) and the data can be obtained only for these values of τ_0 and δ. Thus, using the electron data available at present, the leaky-box model suggests a lifetime

$$\tau_0 = 1.0(+2.0, -0.5) \times 10^7 \text{ yr}\,, \quad \delta = 0.2\text{–}0.7\,, \qquad (23)$$

which is consistent with the value obtained from ^{10}Be data (Garcia-Munoz *et al.* 1977). However, the straight-line spectrum in Figure 9, corresponding to $\tau_0 \geq 3 \times 10^7$ yr cannot be completely excluded. More definitive conclusions would require more accurate data, particularly below 100 GeV and above 1000 GeV. For $\tau_0 < 10^6$ yr, we would need $\delta < 0$, which also disagrees with the heavy primary observations.

It is to be noted that these conclusions are derived by assuming a single-power source spectrum for electrons, and do not depend on the value of the source index γ. However, it is quite probable that the source index for electrons is the same as that for protons, since the observed spectral index for lower energy electrons, 2.8 ± 0.2, is similar to that for protons.

While the leaky-box model provides useful insights into the propagation mechanism, it is perhaps oversimplified. More realistic diffusion models have been investigated by several authors (Jokipii and Meyer 1968; Ramaty *et al.* 1970; Bulanov and Dogel 1974; Ginzburg and Ptuskin 1976; Owens 1976; Owens and Jokipii 1977; Stecker and Jones 1977).

The diffusion model requires specification of the diffusion constant D, the source distribution Q, and the boundary conditions. The diffusion equation governing electron propagation is

$$\frac{\partial J}{\partial t} - \nabla(D\nabla)J - \frac{\partial bE^2 J}{\partial E} = Q\,. \qquad (24)$$

It can be shown that the solutions of the general diffusion equation are linear combinations of the solutions for leaky-box models with different leakage lifetimes, with each contribution weighted appropriately according to the source distribution and boundary conditions (Ginzburg and Ptuskin 1976; Owens 1976).

Jokipii and Meyer (1968) considered the case of a disk-shaped source region, and a diffusion volume without boundary conditions. This corresponds to a large halo, as in the closed galaxy model of Rasmussen and Peters (1975). The model used by Jokipii and Meyer (1968) can be regarded as a linear combination of leaky boxes with lifetimes ranging between $L^2/4D$ and $R^2/4D$, where L and R are, respectively, the

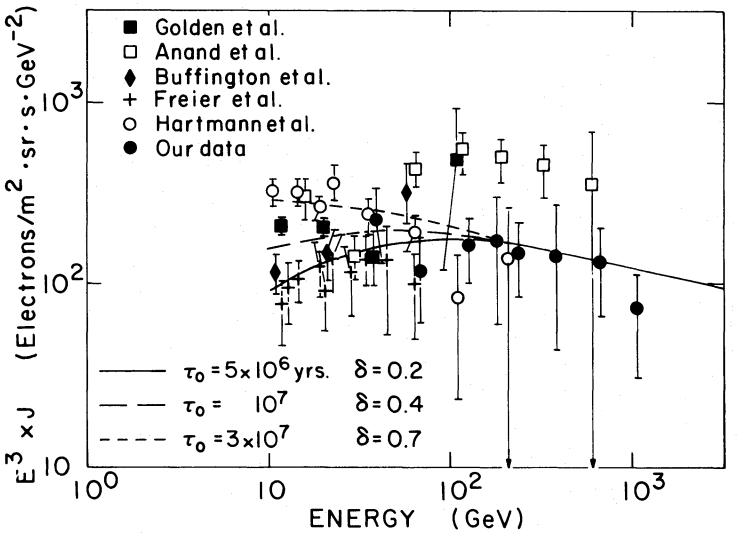

FIG. 9.—Electron spectrum (with vertical scale expanded by a factor of E^3). Curves indicate the spectrum expected from the leaky-box model, for several values of the parameters τ_0 and δ.

thickness and radius of the source disk. The spectrum is expected to be

$$\frac{1}{E^{\gamma+\delta}} \quad \text{for } E \lesssim \frac{4D}{bR^2}, \tag{25}$$

and

$$\frac{1}{E^{\gamma+1}} \quad \text{for } E \gtrsim \frac{4D}{bL^2}. \tag{26}$$

If one takes the commonly accepted galactic dimensions $R = 15$ kpc and $L = 200$ pc, and assumes $D = 10^{28}$ cm^2 s^{-1}; with b as given above, the disk halo model predicts a smooth change of spectral slope over the energy range 0.1–1000 GeV.

The large halo volume used by Jokipii and Meyer is not compatible with the distribution of diffuse γ-rays observed by *COS B* and *SAS 2*, as discussed by Stecker and Jones (1977). Fair agreement is obtained if the halo region is limited to a few kpc in thickness, or if particles in the halo region are prevented from reentering the disk, as in the dynamical halo model (Jokipii 1976; Owens and Jokipii 1977). For the electron flux, a detailed analysis has been performed by the Lebedev group (Bulanov and Dogel 1974; Ginzburg and Ptuskin 1976). If one limits the thickness h of the confinement region as described above without imposing a radial boundary, the solution of the diffusion equation for distance z from the disk plane is

$$J = \sum_{n=0}^{\infty} Q_n \cos\left(\frac{2n+1}{2}\frac{\pi}{h}z\right) \times \exp\left[-\frac{(2n+1)^2}{\tau(1-\delta)bE}\right] \Big/ b(\gamma-1)E^{\gamma+1} \times F\left(1; \frac{\gamma-1}{1-\delta}; \frac{(2n+1)^2}{\tau(1-\delta)bE}\right), \tag{27}$$

where

$$Q_n = \frac{1}{L}\int_{-L}^{+L} \cos\left(\frac{2n+1}{2}\frac{\pi}{h}z'\right) Q(z')dz',$$

$$\tau^{-1} = \frac{\pi^2 D}{4h^2}, \quad D = D_0\left(\frac{E}{5\text{ GeV}}\right)^{\delta}.$$

This is just a linear superposition of leaky boxes, with lifetime parameters varying from L^2/D to h^2/D. The first term dominates, and thus a suitable choice of D gives results similar to those of the leaky-box model. Numerical evaluations of equation (27) are shown in Figure 10, and in fact for $4h^2/\pi^2 D_0 = 4 \times 10^7$ yr, the results show fair agreement with the leaky-box model with $\tau_0 = 10^7$ yr. Thus it is difficult to discriminate between these models using electron-spectrum data alone.

Until now we have discussed only average features of the electron spectrum. However, at energies above 1 TeV, the electron spectrum is expected to show nonstatistical fluctuations due to the influence of a few nearby sources. As shown in equation (13), the electron storage lifetime decreases with increasing energy.

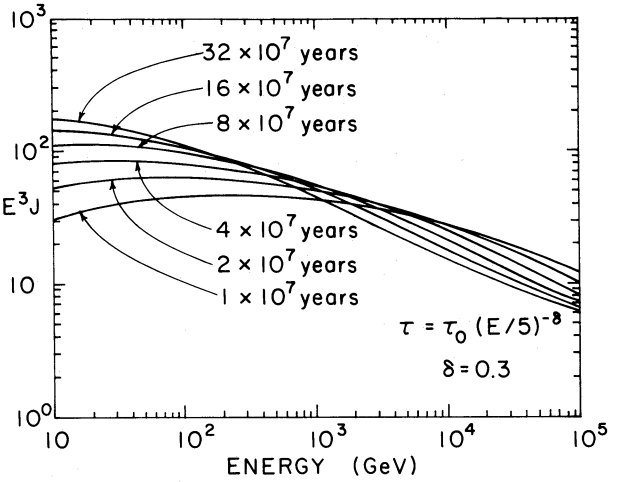

FIG. 10.—Electron spectrum expected from diffusion model, for $\delta = 0.3$ and several values of T_0. The predicted flux J has been multiplied by E^3 to expand the vertical scale.

If we assume a total energy density (for photons and the galactic magnetic field) of 1 eV cm^{-3}, the lifetime at 1 TeV is about 3×10^5 yr. Assuming supernovae to be the sources of cosmic rays, and further assuming that supernovae occur in the galaxy at the rate of one per 30–100 yr (Ilovaisky and Lequeux 1972; Clark and Caswell 1976), one would expect 1000–3000 supernovae within 1 kpc of the solar system in a period of 2×10^7 yr. Such sources would contribute electrons in the 1 GeV range. However, for electrons of energy above 1 TeV, the mean lifetime and propagation distance are expected to be 3×10^5 yr and 300 pc, respectively. Thus only about 2–5 supernovae could be the sources of observed electrons in this energy range. Although the figures given are only illustrative, the conclusion remains that the electron intensity above 1 TeV will show large fluctuations from smooth power-law behavior due to the small number of discrete sources which are capable of contributing to the observed flux. We would therefore expect to observe bumps in the spectrum corresponding to individual sources. This opens up the exciting possibility that, if the electron spectrum measurements can be extended into the TeV region with sufficient precision, we might be able to identify specific sources for the observed high-energy electrons, as discussed by Nishimura *et al.* (1979). Even below 1 TeV, one would expect the electron spectrum to be affected by fluctuations due to these nearby sources. Thus the above discussion of the leaky-box and diffusion models applies to the several hundred GeV region only where such fluctuations are not appreciable.

Additional large emulsion chambers now under analysis will provide improved statistics in the TeV range, and may permit some preliminary conclusions to be drawn regarding nearby sources.

Useful discussions with Drs. S. Hayakawa, Y. Tanaka, K. Sakurai, and H. Hirabayashi are grate-

fully acknowledged. Thanks are also due to Dr. Lou Voyvodic and the staff of Fermilab for assistance with our calibration exposures. We wish to thank R. Kubara, A. Shipley, and the staff of NCAR/NSBF, Palestine, Texas, and S. Ohta, Y. Koma, and the staff of the Sanriku Balloon Flight Center, Japan, for a series of excellent balloon flights. Thanks are due to the Seattle scanning crew, H. Teafer, R. Brzustowicz, D. Kubik, and C. Olason. The work described here was made possible by grants from NASA, NSF (USA), and JSPS (Japan), and by financial support from the Ministry of Education, Japan.

APPENDIX A

SHOWER ENERGY DETERMINATION USING TRACK LENGTH

The concept of track length was first introduced in the one-dimensional electromagnetic shower theory (Tamm and Belenky 1939; Rossi and Greisen 1941; Richards and Nordheim 1948). The track length is given by

$$Z_\pi = \int_0^\infty \Pi(t)dt\,, \tag{A1}$$

where $\Pi(t)$ is the number of electrons in the cascade at depth t. One important feature of Z_π is that it is not subject to statistical fluctuations as are other parameters of the cascade. If energy dissipation occurs only through ionization (since bremsstrahlung, pair production, and the Compton effect represent only exchange of energy between the electron and photon components), the track length should be

$$Z_\pi = E_0/\epsilon\,, \tag{A2}$$

where E_0 is the initial energy and ϵ is the ionization energy loss per unit track length. This is a direct consequence of energy conservation in shower development, and thus the detailed features of cross sections for bremsstrahlung, pair production, and Compton scattering have no effect on Z_π. Another important feature of Z_π is that it is directly proportional to E_0. Other parameters used to estimate E_0 (e.g., $\Pi_{\max}$, the number of shower electrons at shower maximum) have substantial statistical fluctuations and are not directly proportional to E_0.

In the three-dimensional electron shower theory, one can calculate the number of electrons within a circle of radius r at depth t by using the Kamata-Nishimura function (Kamata and Nishimura 1958) and assuming $\epsilon r/K \ll 1$, with the following results:

$$\int_0^r \Pi(E_0, r, t)2\pi r dr = \Pi^{(0)} + \frac{1}{\Omega}\Pi^{(1)} + \frac{1}{\Omega^2}\Pi^{(2)}\cdots;$$

$$\Pi^{(0)} = \frac{1}{2\pi i}\int_{-i\infty}^{+i\infty}\frac{ds}{s}\left(\frac{E_0 r}{K}\right)\Gamma(1-s/2)M\left(\frac{-s}{2}, 0, s\right)\exp(\lambda_1 st) + \cdots,$$

$$\Pi^{(1)} = \frac{1}{4\pi i}\int_{-i\infty}^{+i\infty} ds\left(\frac{E_0 r}{K}\right)^s\Gamma(1-s/2)\left[\psi(1+s/2)M(-1-s/2, 1, s) - \left.\frac{\partial M}{\partial p}\right|_{p=1-s/2}\right]\exp(\lambda_1 st) + \cdots, \tag{A3}$$

with $\epsilon = 7.4$ MeV, $\Omega = 12.9$, $K = 19.6$ MeV for Pb, and where the characteristic scattering energy K, the Moliere parameter Ω, and the function M are as given by Nishimura (1964, 1967). The approximation used for the scattering of shower electrons is similar to the Moliere theory (Moliere 1948), and thus the effects of single, plural, and multiple scattering are included. The track length is derived by integrating (A3) with respect to t, and is given by

$$Z_\pi = \int_0^\infty \Pi dt = \Gamma\left(\frac{1}{2}\right)\frac{E_0 r}{K}\left[M\left(\frac{1}{2}, 0, 1\right) + \frac{1}{2}\frac{1}{\Omega}\psi\left(\frac{1}{2}\right)M\left(-\frac{3}{2}, 1, 1\right) - \left.\frac{\partial M(p, 1, 1)}{\partial p}\right|_{p=0}\right]. \tag{A4}$$

Unlike the one-dimensional case, the track length in the three-dimensional theory may exhibit fluctuations from shower to shower, since not all shower particles are included. However, fluctuations caused by displacement of the shower starting point have no effect, and the track length is still directly proportional to the primary energy.

The inhomogeneous structure of our emulsion chambers is approximately taken into account by introducing an appropriate value for the radiation length. For $r = 100$ μm, the track length is then

$$Z_\pi = 1.1E_0\,, \tag{A5}$$

where E_0 is in GeV. The results of a Monte Carlo calculation for the same chamber configuration (Taira 1979) agree with equation (A5) within several percent. The fluctuations in the energy determined from Z_π, $\Pi_{\max}$, or the number of tracks at a given depth in the chamber can be investigated using the Monte Carlo method. Our calculations show that in the energy range of interest, the standard deviation in the energy determined from Z_π is about 70% of that calculated using $\Pi_{\max}$, and about 50% of that calculated from the number of tracks at a given depth. Figure 3

shows the observed shower development in calibration chambers of design identical to the balloon-flight chambers, exposed to 50, 100 and 300 GeV electrons electrons at Fermilab. Also shown are the corresponding theoretical curves. The experimental data agree with the calculated values within 10%. We therefore used

$$Z_\pi = 1.10E_0\,, \quad E_0 \text{ in GeV}\,, \tag{A6}$$

obtained from the Fermilab calibration data, for determining the energies of primary electrons in this experiment.

APPENDIX B

ATMOSPHERIC CORRECTIONS

In balloon flight experiments, corrections to the measured cosmic-ray electron spectrum are necessary because of the residual overlying atmosphere. Two effects may require significant correction: energy loss by primary electrons due to bremsstrahlung in the atmosphere, and production of secondary electrons via γ-rays from neutral pion decay.

One might assume that the bremsstrahlung energy loss to each electron is simply given by $dE/dt = -E$, so that

$$E = E_0 e^{-t}\,, \tag{B1}$$

where E_0 is the energy at the top of the atmosphere and t is measured in radiation lengths. While equation (B1) gives the most likely energy loss for a beam which is monoenergetic, the best estimate of E_0 should be smaller if the input spectrum is steeply sloped, because of the broad distribution of produced photons described by the Bethe-Heitler formula. A realistic estimate can be obtained using the results of the cascade theory, as follows.

Let $\pi(E, t)$ be the differential energy spectrum of electrons, and $\Phi(E, W)dW/E$ be the probability that an electron of energy E will emit a γ-ray of energy W per radiation length. Then

$$\frac{\partial \Pi(E, t)}{\partial t} = -\Pi(E, t)\int_0^E \Phi_0\left(\frac{W}{E}\right)\frac{dw}{E} + \int_0^\infty \Pi(E', t)\Phi_0\left(\frac{E' - E}{E'}\right)\frac{dE'}{E'}\,. \tag{B2}$$

Using the Bethe-Heitler formula, an exact solution can be derived by the method of Mellin transforms, with boundary condition at $t = 0$

$$\pi(E, 0) = \frac{1}{E^{s+1}}\,. \tag{B3}$$

The solution is

$$\pi(E, t) = \frac{e^{-A(s)t}}{E^{s+1}}\,, \tag{B4}$$

where

$$A(s) = \int_0^1 \frac{1 - (1 - v)^s}{v}\Phi(v)dv = 1.36\frac{d\Gamma(s + 2)}{ds} - \frac{1}{(s + 1)(s + 2)} - 0.075\,. \tag{B5}$$

From equation (B4), the energy-loss correction due to the overlying atmosphere is calculated to be

$$E_0 = Ee^{A(s)t/s} \tag{B6}$$

compared to the correction factor based on the simple energy-loss picture,

$$E_0 = Ee^t\,. \tag{B7}$$

The ratio of the two corrections is $\exp\{[A(s)/s - 1]t\}$. Figure 11 shows numerical evaluations indicating the percentage by which (B7) overestimates the energy correction.

The number of secondary electrons produced by atmospheric γ-rays can be estimated as follows. Let $\gamma(W, t)$ be the differential spectrum of atmospheric γ-rays, and let $\psi_0(W, E)dE/W$ be the probability per radiation length that a γ-ray of energy W will produce a pair of electrons of energies E and $W - E$. If the depth is small compared to 1 r.l., the γ-ray flux is approximately

$$\gamma(W, t) = \gamma_0(W)t\,. \tag{B8}$$

Then the number of secondary electrons produced by these γ-rays is given by

$$\pi(E, t) = 2\int_E^\infty \gamma_0(W)\psi_0(E/W)\frac{dE}{W}\int_0^t tdt\,. \tag{B9}$$

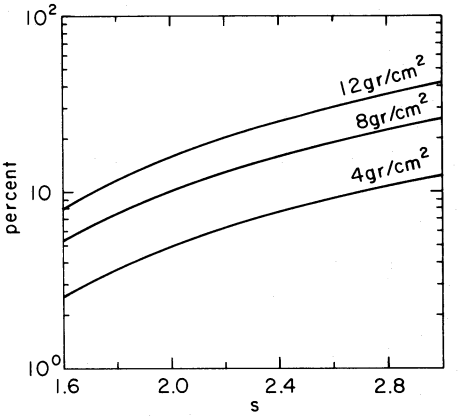

FIG. 11.—Percentage error in simple energy-loss estimate of energy correction for residual atmosphere, as a function of the primary integral spectrum slope parameter s, for 4, 8, and 12 g cm^{-2} overburden.

If the energy spectrum of γ-rays has the form dW/W^{s+1} (as is in fact observed), the flux of secondary electrons is

$$\pi(E, t) = B(s)\gamma_0(W)t^2/2 , \tag{B10}$$

where

$$B(s) = 2\int_0^1 U^s\psi_0(U)dU = 2\left[\frac{1}{s+1} - \frac{1.36}{(s+2)(s+3)}\right]. \tag{B11}$$

Using the observed γ-ray flux given in formula (4) in § III*b*, the secondary electron flux at depth $t = 4\ g\ cm^{-2}$ is

$$\pi(E, t) = 3.7 \times 10^{-6}(100\ \text{GeV}/E)^{2.75\pm0.02}/\text{m}^2\ \text{sr s GeV} , \tag{B12}$$

which is to be compared with the observed electron flux

$$J_e = 1.6 \times 10^{-4}(100\ \text{GeV}/E)^{3.3\pm0.2}/\text{m}^2\ \text{sr s GeV} ,$$

Thus the secondary electrons comprise a few percent of the observed flux in the 100 GeV region at $t = 4$ g cm^{-2} (the depth at which the 1976 exposure took place).

The fraction of secondary electrons present will increase in the TeV region due to the steep primary spectrum. However, in this energy range the angular separation of the pair becomes very small, and one would expect to see both particles as parallel showers within a few cm of one another in the emulsion chamber; such events are rejected. Thus the contamination of our data sample by secondary electrons should be negligible even in the high-energy region.

REFERENCES

Anand, K. C. 1973, Ph.D. thesis, Tata Institute, Bombay.
Anand, K. C., Daniel, R. R., and Stephens, S. A. 1968, *Phys. Rev. Letters*, **20**, 764.
———. 1970, *Acta Phys. Acad. Sci. Hungary*, Vol. **29**, Suppl. 1, p. 229.
———. 1973, *Proc. 13th Internat. Cosmic Ray Conf.*, **1**, 355.
Badhwar, G. D., Stephens, S. A., and Golden, R. L. 1977, *Phys. Rev.*, **15**, 820.
Badhwar, G. D., Daniel, R. R., and Stephens, S. A. 1977, *Nature*, **265**, 424.
Bennett, K., *et al.* 1977, *Astr. Ap.*, **56**, 469.
Bleeker, J. A. M., *et al.* 1965, *Proc. 9th Internat. Cosmic Ray Conf.*, **1**, 327.
Buffington, A., *et al.* 1975, *Ap. J.*, **199**, 669.
Bulanov, S. V., and Dogel, V. A. 1974, *Ap. Space Sci.*, **28**, 305.
Caldwell, J. H. 1977, *Ap. J.*, **218**, 269.
Clark, D. H., and Caswell, F. L. 1976, *M.N.R.A.S.*, **174**, 267.
Cowsik, R., and Lee, M. A. 1979, *Ap. J.*, **228**, 297.
Cowsik, R., and Mitteldorf, J. 1974, *Ap. J.*, **189**, 51.
Cowsik, R., and Wilson, L. W. 1973, *Proc. 13th Internat. Cosmic Ray Conf.*, **1**, 500.
Critchfield, C. L., *et al.* 1952, *Phys. Rev.*, **79**, 204.
Daniel, R. R., and Stephens, S. A. 1965, *Phys. Rev. Letters*, **15**, 769.
Earl, J. A. 1961, *Phys. Rev. Letters*, **6**, 193.
Fichtel, C. E., *et al.* 1975, *Ap. J.*, **198**, 163.
Freier, P. S., Gilman, C., and Waddington, C. J. 1977, *Ap. J.*, **213**, 588.
Fuchi, H., *et al.* 1978, *Nuovo Cimento*, **45**, 471.
Fujimoto, Y., *et al.* 1960, *Proc. 6th Internat. Cosmic Ray Conf.*, **1**, 41.
Garcia-Munoz, M., *et al.* 1977, *Ap. J. (Letters)*, **217**, 131.
Ginzburg, V. L., and Ptuskin, V. S. 1976, *Rev. Mod. Phys.*, **48**, 161.
Golden, R. L., *et al.* 1977, *Proc. 15th Internat. Cosmic Ray Conf.*, **1**, 404.
———. 1979, private communication.
Hartmann, G., Muller, D., and Prince, T. 1977, *Phys. Rev. Letters*, **38**, 1368.
Hirabayashi, H. 1974, *Pub. Astr. Soc. Japan*, **26**, 263.
———. 1979, private communication.
Ilovaisky, S. A., and Lequeux, J. 1972, *Astr. Ap.*, **18**, 169.
Jokipii, J. R. 1976, *Ap. J.*, 208, 906.
Jokipii, J. R., and Meyer, P. 1968, *Phys. Rev. Letters*, **20**, 752.
Juliusson, E. *et al.* 1975, *Proc. 14th Internat. Cosmic Ray Conf.*, **2**, 653.
Kamata, K., and Nishimura, J. 1958, *Suppl. Progr. Theor. Phys. Japan*, **6**, 93.
Kaplon, M. F., *et al.* 1952, *Phys. Rev.*, **85**, 295.
Konishi, S., *et al.* 1976, *Phys. Rev.*, **13**, 1826.
Lezniak, J. A., *et al.* 1977, *Proc. 15th Internat. Cosmic Ray Conf.*, **1**, 237.
Meegan, C. A., and Earl, J. A. 1975, *Ap. J.*, **197**, 219.

Meyer, P., and Vogt, R. 1961, *Phys. Rev. Letters*, **6**, 193.
Minakawa, O., *et al.* 1958, Nuovo Cimento Suppl., **8**, 761.
Moliere, G. 1948, *Z. Naturforsch.* **3A**, 78.
Müller, D., and Meyer, P. 1973, *Ap. J.*, **186**, 841.
Murakami, K., *et al.* 1977, *Proc. 15th Internat. Cosmic Ray Conf.*, **6**, 143.
———. 1979, *Proc. 16th Internat. Cosmic Ray Conf.*, **1**, 484.
Nishimura, J. 1961, *J. Phys. Soc. Japan* (*Proc. 7th Internat. Cosmic Ray Conf.*, (Suppl. A-III), **17**, 427.
———. 1964, *Progr. Theor. Phys. Japan*, *Suppl.*, **32**, 72.
———. 1967, *Handbuch der Physik*, XLVI/2, (Berlin: Springer), p. 1.
Nishimura, J., *et al.* 1970, *Proc. 11th Internat. Cosmic Ray Conf.*, **1**, 239.
———. 1979, *Proc. 16th Internat. Cosmic Ray Conf.*, **1**, 478.
Ohta, I. 1971, *Prog. Theor. Phys. Suppl.*, **47**, 271.
Ohta, I., *et al.* 1979, *Nucl. Inst. Methods*, **161**, 35.
Ormes, J., and Freier, P. S. 1978, *Ap. J.*, **222**, 471.
Orth, C. D., and Buffington, A. 1976, *Ap. J.*, **206**, 312.
Orth, C. D. *et al.* 1978, *Ap. J.*, **226**, 1147.
Owens, A. J. 1976, *Ap. Space Sci.*, **40**, 357.
Owens, A. J., and Jokipii, J. R. 1977, *Ap. J.*, **215**, 677.
Paul, J. A., *et al.* 1978, *Astr. Ap.* (*Letters*), **63**, L31.
Prince, T. A. 1979, *Ap. J.*, **227**, 676.
Ramaty, R. 1974, *High Energy Particles and Quanta in Astrophysics*, ed. F. B. MacDonald and C. E. Fichtel (Cambridge: MIT Press), p. 122.
Ramaty, R., *et al.* 1970, Phys. Rev. Letters, **24**, 913.
Rasmussen, I. L., and Petters, B. 1975, *Nature*, **258**, 412.
Reames, V. V. 1974, *High Energy Particles and Quanta in Astrophysics*, ed. F. B. MacDonald and C. E. Fichtel (Cambridge: MIT Press), p. 54.
Richards, J. A., and Nordheim, W. 1948, *Phys. Rev.*, **74**, 1106.
Rossi, B., and Greisen, K. 1941, *Rev. Mod. Phys.*, **13**, 240.
Rubtsov, V. I. 1965, *Proc. 9th Internat. Cosmic Ray Conf.*, **1**, 324.
Rubtsov, V. I., and Zatsepin, V. I. 1968, *Canadian J. Phys.*, **46**, 8518.
Ryan, M. J., *et al.* 1972, *Phys. Rev. Letters*, **28**, 985.
Sato, Y., *et al.* 1976, *J. Phys. Soc. Japan*, **41**, 1821.
Shen, C. S. 1970, *Ap. J.* (*Letters*), **162**, 181.
Silverberg, R. 1973, *J. Geophys. Rev.*, **78**, 7165.
———. 1976, *J. Geophys. Res.*, **81**, 3944.
Silverberg, R. F., and Ramaty, R. 1973, *Nature*, **243**, 134.
Smith, L. H., *et al.* 1973, *Ap. J.*, **180**, 987.
Stecker, F. W., and Jones, F. C. 1977, *Ap. J.*, **217**, 843.
Stephens, S. A. 1970, *Proc. Indian Acad. Sci.*, **62**, 214.
Taira, T. 1979, private communication.
Takahashi, Y., Iwai, J., and Ohta, I. 1977, *Proc. 15th Internat. Cosmic Ray Conf.*, **7**, 408.
Tamm, I., and Belenky, S. 1939, *J. Phys. USSR*, **1**, 177.
Tasaka, S. 1979, private communication.
Webber, W. R. 1973, *Proc. 13th Internat. Cosmic Ray Conf.*, **5**, 3568.

E. Aizu, M. Fujii, H. Hiraiwa, T. Kobayashi, J. Nishimura, K. Niu, I. Ohta, and T. Taira: Institute of Space and Aeronautical Science, Komaba, Meguro-ku, Tokyo 153, Japan

R. L. Golden: Physical Sciences Laboratory, New Mexico State University, Las Cruces, NM 88003

T. A. Koss, J. J. Lord, and R. J. Wilkes: Department of Physics FM-15, University of Washington, Seattle, WA 98195